Local Density of States in Zero-Dimensional Semiconductor Structures

K. Kanisawa,[1] M. J. Butcher,[1,2] Y. Tokura,[1] H. Yamaguchi,[1] and Y. Hirayama[1,3]

[1]*NTT Basic Research Laboratories, NTT Corporation, 3-1 Wakamiya, Morinosato, Atsugi, Kanagawa, 243-0198, Japan*
[2]*School of Physics and Astronomy, University of Nottingham, Nottingham NG7 2RD, United Kingdom*
[3]*CREST-JST, 4-1-8 Honmachi, Kawaguchi, Saitama, 331-0012, Japan*
(Received 6 February 2001; published 22 October 2001)

The local density of states (LDOS) within tetrahedral InAs structures, formed at the surface of InAs/GaAs(111)A, has been characterized using low-temperature scanning tunneling microscopy. The LDOS of the lowest four zero-dimensional (0D) discrete levels have been imaged in structures with a comparable size to the electron wavelength. The LDOS inside the structures is observed to be higher than that of the surrounding area at intervals of the level separation. This feature indicates the singularity of the LDOS close to the 0D resonant levels.

DOI: 10.1103/PhysRevLett.87.196804 PACS numbers: 73.21.La, 68.37.Ef, 73.20.–r, 73.22.–f

Zero-dimensional (0D) semiconductor structures have attracted much attention towards understanding fundamental 0D physics and device applications. The properties of 0D states have been studied using a single quantum dot (QD) [1–3]. The scanning tunneling microscope (STM) is an ideal tool for such characterization as it is capable of atomic-scale spatial resolution [4–6]. Spectroscopic studies have been reported recently [7,8]. However, individual 0D eigenstates have not yet been studied by local density of states (LDOS) imaging.

In this Letter, we report LDOS imaging of nanometer-scale tetrahedral InAs structures. The experiments were undertaken using a low-temperature STM (LT-STM). Our analysis shows that each image relates to a discrete 0D eigenstate confined to the tetrahedron.

An undoped InAs thin film, thicker than 100 nm, was grown on an n-type GaAs(111)A substrate by molecular beam epitaxy [9]. The surface is atomically smooth with an accumulation of two-dimensional (2D) electrons [10,11]. This is different from that of the cleaved n-InAs(110) surface, where standing waves due to three-dimensional (3D) electrons are imaged [12]. After the growth, the sample was transferred to the LT-STM in ultrahigh vacuum and cooled to 5.3 K. A small modulation (5 mV rms, 600 Hz) was applied to the bias voltage V during the topographic imaging. The differential conductance (dI/dV) signal was simultaneously mapped using a lock-in amplifier to obtain the LDOS distribution [13].

At the InAs(111)A surface, triangular defects are observed [Fig. 1(a)]. The defects are of fractional (1/3 or 2/3) monolayer height difference and are the surfaces of stacking fault tetrahedrons (SFT's) [14]. They consist of nanometer-scale InAs crystal. A strain relaxation mechanism between the InAs thin film and the GaAs substrate results in the formation of such SFT's. The SFT is surrounded by the (111)A surface and three triangular {111}-stacking fault planes below the surface [Fig. 1(b)]. Each intersection of these planes is a Lomer-Cottrell sessile (or Frank partial) dislocation [14]. The stacking fault plane has a bond configuration that is the same as the wurtzite structure and is a crystal phase boundary. The bonds in the plane have a different polarization to those in the zinc-blende structure. The sessile dislocation is known to have dangling bonds and can act as a charged defect array [15]. The stacking fault plane and the dislocation give rise to a scattering potential. Thus, the SFT can be considered as a translucent shell for electrons where 0D features are expected. It should be noted that the SFT is separated from the surface electron accumulation layer by an atomically thin boundary. Also, the confined states for such an SFT would not be the same as for the bound states of a QD. This is because the DOS is determined through a resonant tunneling to the surface conductive layer.

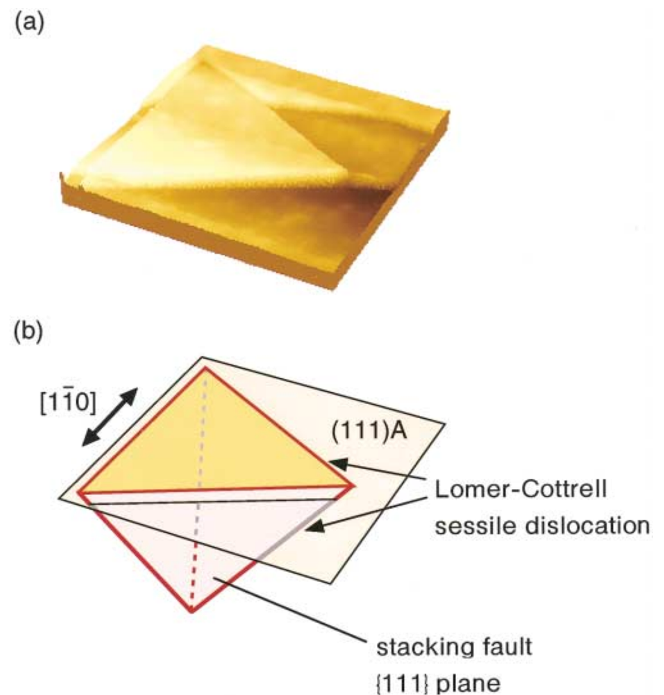

FIG. 1 (color). (a) An STM image of a triangular shaped defect at the epitaxial InAs surface. Image size is 134 nm × 134 nm. (b) Schematic illustration of the stacking fault tetrahedron (SFT).

 © 2001 The American Physical Society

Figure 2(a) shows an STM image. The corresponding dI/dV image shows circular patterns around points P1 and P2, regular patterns within the large triangle (L), and a toroidal pattern within the smaller triangle (S). P1 and P2 arise due to a threading dislocation. As the dislocation lies along the inclined {111}-gliding plane, the standing wave reveals anisotropic features. The calculated electron coherence length is about 400 nm, considering the thermal broadening of $|\mathbf{k}_{\|}|$ ($\mathbf{k}_{\|}$: the wave vector parallel to the surface) and for a temperature $T = 5.3$ K [16]. The oscillatory features are observed up to a 100 nm from the scatterers. This is because the bias modulation is much larger than $k_B T$ (k_B: Boltzmann's constant).

The energy band profile at the surface is illustrated in Fig. 2(b). The eigenstates of an electron in an equilateral triangle and a tetrahedron have been calculated [17]. However, a numerical calculation is necessary for the present system due to the band bending at the surface and near the edge of the SFT. The quantitative boundary conditions of the SFT are unknown. Therefore we have used a simplified model that the imaged LDOS of 0D resonant states can be approximated by the 2D states confined to a triangular boundary. This is because the SFT has a comparable size to the thickness of the electron accumulation layer, where the SFT is in the electric field vertical to the surface due to the band bending. Since the LDOS at the edge of the triangle shows a density peak, the dislocation there is expected to act as a donor-type defect array [15]. The boundary is assumed to be made of a positively charged hard wall with downward band bending [Fig. 2(c)].

The energy levels, and the amplitude of the corresponding probability distribution, were calculated within the SFT. This was undertaken by solving Schrödinger's equation with a tight-binding approximation for a triangular lattice. The calculation was performed where band bending is expressed in a formula proportional to $-(l - s)^2$ within the triangle, and with a condition $E \equiv 0$ eV at the center. Here l and s are the distance from the center to the side and the distance from each point to the nearest side. We used a potential difference of about 0.2 ± 0.1 eV between the center and at the wall. The electron effective mass m^* is $0.043m_0$, which is equivalent to that of the surrounding 2D states [10,11].

For the case of a large SFT [L in Fig. 2(a)] with a side length (97.7 nm) $\gg$ electron wavelength λ (17.7 nm at $V = +0.10$ V), the SFT can effectively act as a 2D quantum cage [Fig. 2(b)]. The corresponding dI/dV image in Fig. 2(a) shows the periodic arrangement of symmetric patterns within the SFT. For the case of a small SFT [S in Fig. 2(a)] the side length (17.3 nm) $\approx \lambda$. Figure 3

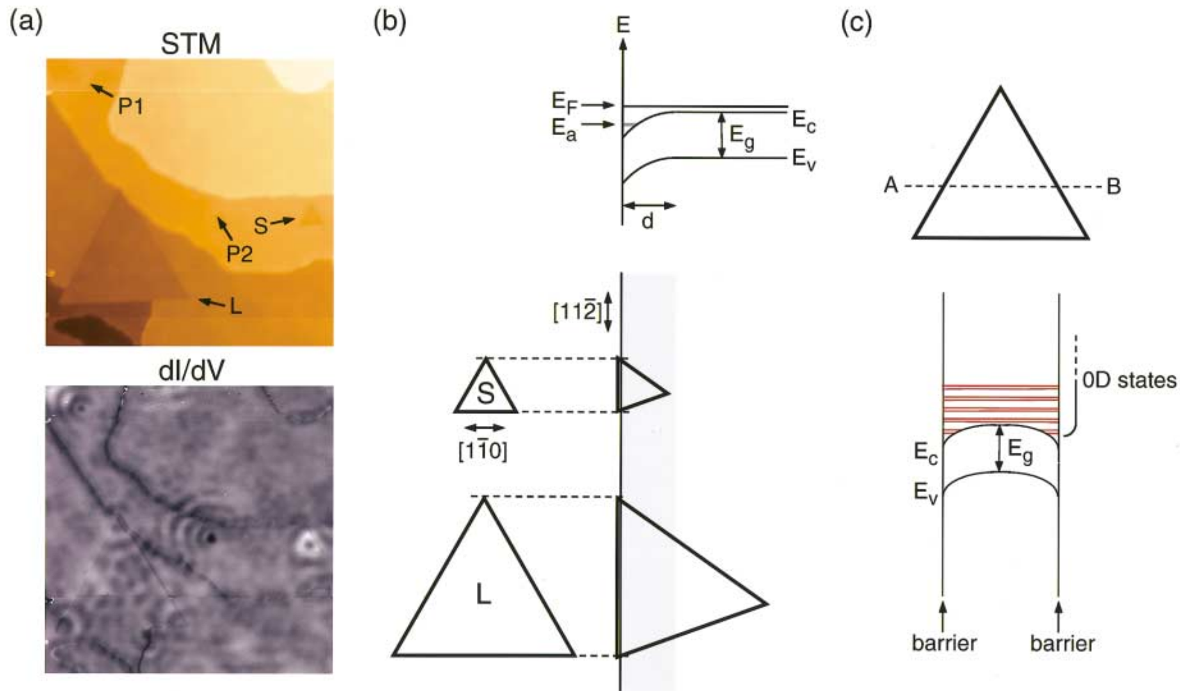

FIG. 2 (color). (a) STM and dI/dV images of the epitaxial InAs surface ($V = +0.06$ V, $I = 0.24$ nA). Image size is 214.4 nm × 214.4 nm. Two isolated point defects (P1 and P2), a small SFT (S), a large SFT (L), monolayer step edges, and the corresponding LDOS are visible. A bright feature within S is observed. The brighter regions are due to a higher LDOS. (b) Schematical illustration of a cross-sectional view of band bending near the surface. Effect of electron accumulation layer (thickness $d \approx 20$ nm) to L and S are also shown as a gray-colored region. Equilateral triangles show the top view of SFT's. E_F, E_a, and E_g are the Fermi level, the 2D subband level, and the band gap of InAs (0.42 eV at 5.3 K), respectively. (c) Detailed cross-sectional band profile of an SFT along the A-B line is shown. Discrete 0D levels are also illustrated. An infinitely high potential with a positive charge is assumed at the boundaries considering the character of the SFT boundary. (See text for discussion.)

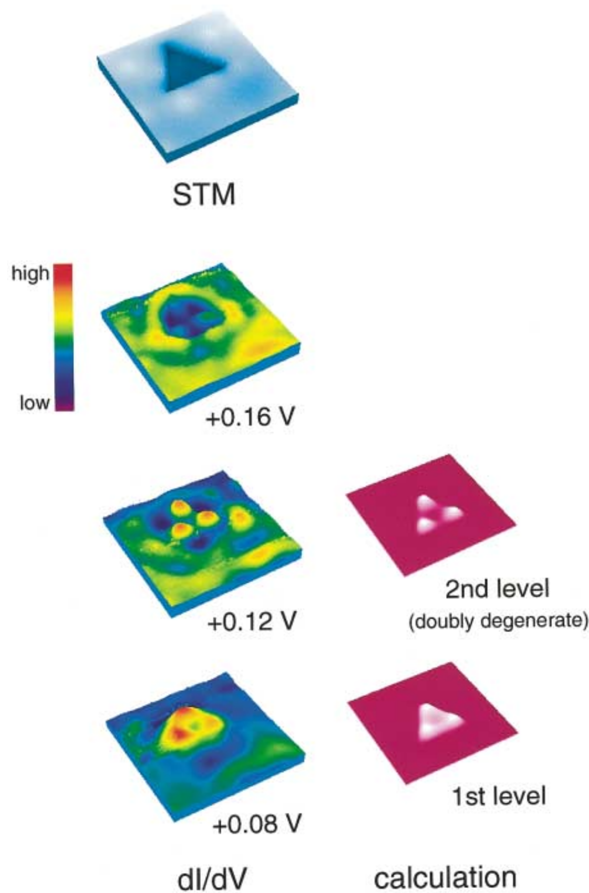

FIG. 3 (color). An STM image of an SFT on the InAs(111)A surface ($V = +0.12$ V, $I = 0.24$ nA). Image size is 40.2 nm $\times$ 40.2 nm. The SFT has a side length of 17.3 nm. Spatial images of the LDOS are shown in the dI/dV images at $V = +0.08$, $+0.12$, and $+0.16$ V. Blue to red corresponds to an increasing LDOS. The theoretically calculated first and second energy level probability distributions are also shown. The calculated probability distributions are normalized by integrating the probability over the entire SFT. Brighter regions correspond to higher probability.

shows magnified images for SFT S. When the electron energy E was increased, in the unoccupied ($V > 0$) sample DOS region, the average DOS surrounding the SFT gradually increased. This reflects the constant 2D DOS on the background 3D DOS ($\propto\sqrt{E}$). However, the dI/dV images show that there are bias voltage conditions where the intensity of the internal DOS features of the SFT is remarkably higher [Figs. 2(a) and 3 at $V = +0.08$ and $+0.12$ V] or lower (Fig. 3 at $V = +0.16$ V) than those outside. This was not observed for the LDOS intensity, caused by the Friedel oscillations, around P1 and P2. The intensity behavior within the SFT is due to the singularity of the 0D DOS. When imaging is performed close to 0D resonant level, a maximum intensity is observed.

According to our calculations, the observed pattern at $+0.08$ V corresponds to LDOS of first level (ground state) which is capable of holding a maximum of 2 electrons. At $V = +0.12$ V, the LDOS is the probability distribution for the second level that consists of two degenerate states. The LDOS pattern therefore results from the sum of these two degenerate states which are able to accept a maximum of 4 electrons. The energy separation between the first and the second levels is calculated to be 0.066 eV which is comparable with the energy difference of 0.04 eV in Fig. 3. The bias difference is larger than the bias modulation. The energy separation between the second and the third levels is calculated to be 0.21 eV, which is much larger than the energy difference of 0.04 eV. Therefore, the results show that the patterns are the LDOS of discrete 0D levels at $V = +0.08$ and $+0.12$ V (close to resonant conditions). The pattern at $+0.16$ V is a tail of the closest LDOS of the second level (distant from resonant condition). As we can observe the first two 0D states at $V > 0$, the potential height of the barrier can be expected to be at least several 100 meV.

To probe higher energy levels, we examined a slightly larger SFT (Fig. 4). The dI/dV images at $+0.10$ and $+0.12$ V again excellently coincide with the discrete third and fourth 0D states calculated. The third and the fourth energy levels consist of one discrete and two degenerate states, respectively. The energy difference of 0.02 eV is comparable with the calculated separation of 0.014 eV between the two levels. Our model for the observed LDOS is, therefore, in good agreement with the experimental results, and we can attribute each observed LDOS to each discrete 0D eigenstate for the lowest four energy levels.

Figure 5 shows an STM and dI/dV images of a medium-sized SFT. Threefold symmetric LDOS peaks

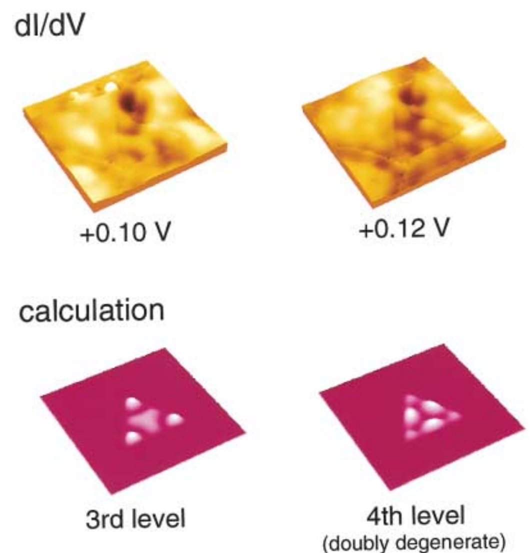

FIG. 4 (color). The dI/dV images and calculation results for an SFT with a side length of 33.9 nm. The images taken at $+0.10$ V ($I = 0.19$ nA) and $+0.12$ V ($I = 0.26$ nA) are attributed to the third and fourth energy levels, respectively. The calculated probability distributions are normalized by integrating the probability over the entire SFT. Brighter regions correspond to higher probability.

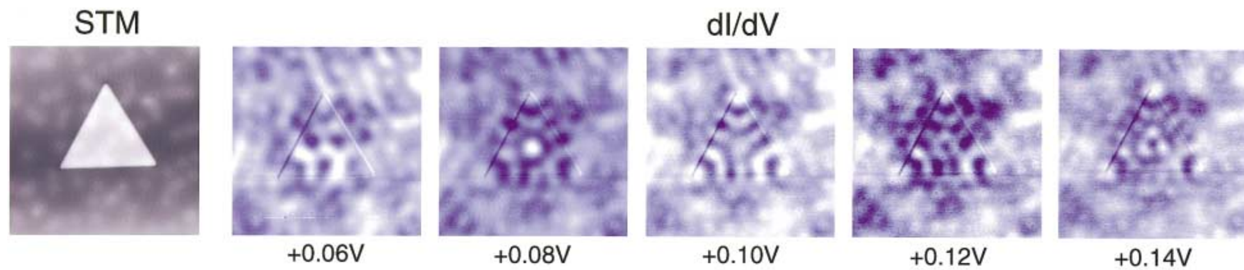

FIG. 5 (color). An STM and the dI/dV images of an SFT with a side length of 48.7 nm at bias voltages from +0.06 to +0.14 V ($I = 0.20$ nA). Each image size is 93.8 nm × 93.8 nm.

are always observed. Each dI/dV image is likely to be a convolution of two or three 0D states. This is because a larger modulation amplitude than the energy separation between states is used. At the nth level (roughly $10 \leq n$), the energy separation becomes smaller than 0.01 eV. However, qualitative tendency in the bias-dependent nodal features of the LDOS is still consistent with our calculation.

In summary, the characterization of the LDOS in 0D semiconductor structures has been achieved using LT-STM. The LDOS in small SFT's can be attributed to discrete 0D eigenstates. These features have been consistently explained using a simple model. As the size of the SFT's is comparable with artificial atoms, this may contribute to the investigation of 0D states in nanostructures.

This study was partly supported by the NEDO collaboration program (NTDP-98) and the Japan Society for the Promotion of Science ("Research for Future" Programs JSPS-RFTF96P00103). M. J. B. thanks EPSRC.

[1] L. P. Kouwenhoven, T. H. Oosterkamp, M. W. S. Danoesastro, M. Eto, D. G. Austing, T. Honda, and S. Tarucha, Science **278**, 1788 (1997), and references therein.
[2] J.-Y. Marzin, J.-M. Gérard, A. Izraël, D. Barrier, and G. Bastard, Phys. Rev. Lett. **73**, 716 (1994), and references therein.
[3] Y. Toda, S. Shinomori, K. Suzuki, and Y. Arakawa, Appl. Phys. Lett. **73**, 517 (1998).
[4] M. F. Crommie, C. P. Lutz, D. M. Eigler, and E. J. Heller, Physica (Amsterdam) **83D**, 98 (1995), and references therein.
[5] J. Li, W.-D. Schneider, R. Berndt, and S. Crampin, Phys. Rev. Lett. **80**, 3332 (1998).
[6] T. Yokoyama and K. Takayanagi, Phys. Rev. B **59**, 12 232 (1999).
[7] E. E. Vdovin, A. Levin, A. Patanè, L. Evans, P. C. Main, Yu. N. Khanin, Yu. V. Dubrovskii, M. Henini, and G. Hill, Science **290**, 122 (2000).
[8] B. Grandidier, Y. M. Niquet, B. Legrand, J. P. Nys, C. Priester, D. Stiévenard, J. M. Gérard, and V. Thierry-Mieg, Phys. Rev. Lett. **85**, 1068 (2000).
[9] H. Yamaguchi, M. R. Fahy, and B. A. Joyce, Appl. Phys. Lett. **69**, 776 (1996).
[10] K. Kanisawa, M. J. Butcher, H. Yamaguchi, and Y. Hirayama, in *Proceedings of the 25th International Conference on the Physics of Semiconductors, Osaka, Japan, 2000,* edited by N. Miura and T. Ando, Springer Proceedings in Physics Vol. 87 (Springer-Verlag, Berlin, Heidelberg, 2001), Pt. I, p. 427.
[11] K. Kanisawa, M. J. Butcher, H. Yamaguchi, and Y. Hirayama, Phys. Rev. Lett. **86**, 3384 (2001).
[12] Chr. Wittneven, R. Dombrowski, M. Morgenstern, and R. Wiesendanger, Phys. Rev. Lett. **81**, 5616 (1998).
[13] J. Li, W.-D. Schneider, and R. Berndt, Phys. Rev. B **56**, 7656 (1997).
[14] D. Hull and D. J. Bacon, *Introduction to Dislocations* (Pergamon Press, Oxford, 1984), Chap. 5.
[15] Yu. A. Osip'yan, V. F. Petrenko, A. V. Zaretskii, and R. W. Whitworth, Adv. Phys. **35**, 115 (1986).
[16] Y. Hasegawa and Ph. Avouris, Phys. Rev. Lett. **71**, 1071 (1993).
[17] H. R. Krishnamurthy, H. S. Mani, and H. C. Verma, J. Phys. A **15**, 2131 (1982).